Progress in Medical Devices
ISSN: 2957-5478

Zentime

Research Article https://doi.org/10.61189/828047gamhgw

A method for predicting the outcome of PD1/PD-L1 inhibitors in non-small cell lung cancer

Wensong Yan[1], Shiju Yan[1], Yunhua Xu[2]

[1]School of Health Science and Engineering, University of Shanghai for Science and Technology, Shanghai 200093, China. [2]Department of Oncology, Shanghai Chest Hospital, Shanghai 200030, China.

Corresponding author: Shiju Yan.

Declaration of conflict of interest: None.

Received January 13, 2025; Accepted April 15, 2025; Published December 31, 2025

Highlights

- This study introduces a novel method to predict the efficacy of PD1/PD-L1 inhibitors in non-small cell lung cancer by extracting radiomic features from pre-treatment and post-treatment CT images.
- Integrating biological features and radiomic features enhances predictive performance.
- The newly proposed segmentation model achieved a dice coefficient of 90.09%, enabling accurate lesion segmentation.

Abstract

Objective: To propose a method for predicting immunotherapy outcome in non-small cell lung cancer based on computed tomography images before and after treatment. **Methods:** An improved U-net model incorporating Efficient Channel Attention was used to segment lesions. Radiomic features of lesions were extracted using PyRadiomics package and combined with biological indicators. Feature selection and dimensionality reduction were performed using linear discriminant analysis and Pearson correlation algorithms. A support vector machine was used to establish the predictive model. **Results:** The proposed segmentation model achieved a Dice coefficient of 90.09%, a positive predictive value of 89.23%, and an intersection over union of 82.15%, outperforming mainstream segmentation models. The proposed predictive model achieved an area under the curve of 85.05%, accuracy of 77.59%, specificity of 81.68% and sensitivity of 73.52%, all superior to models based solely on single-time computed tomography images or lacking biological features. **Conclusion:** The proposed method provides an effective approach for predicting the efficacy of immunotherapy in non-small cell lung cancer patients and offers a valuable tool to support clinical decision-making.

Keywords: Immunotherapy, medical image segmentation, non-small cell lung cancer, machine learning, feature engineering

Introduction

Lung cancer is a prevalent malignancy worldwide, with non-small cell lung cancer (NSCLC) accounting for 80%-85% of all lung cancer cases, making its treatment a critical focus in the medical field [1, 2]. Studies have demonstrated that immune checkpoint inhibitors (ICIs) significantly enhance the objective response rate and prolong the survival of lung cancer patients. As a result, PD-L1 testing is clinically recommended for NSCLC patients to identify those who may benefit from immunotherapy [3, 4]. However, even PD-L1-negative patients have shown benefits from ICIs, suggesting that the efficacy of ICIs in NSCLC is not universally predictable [5, 6]. Additionally, PD-L1 testing, being invasive, is not universally suitable [7]. Therefore, developing a model capable of accurately and non-invasively predicting the efficacy of lung cancer immunotherapy is crucial for optimizing treatment strategies and improving patient outcomes. The segmentation of lesion areas and the selection of relevant features are critical components of this process.

The U-Net network proposed by Ronneberger et al. has been widely used in medical image processing due to its superior performance and

Address correspondence to: Shiju Yan, School of Health Sciences and Engineering, University of Shanghai for Science and Technology, No.580 Jungong Road, Shanghai 200093, China. Tel: +86-18217617984. E-mail: yanshiju@usst.edu.cn.

relatively low training sample requirements [8]. The U-Net++ proposed by Zong et al. enhanced feature map connectivity across different resolutions, enabling the capture of higher-level features and improving segmentation performance [9]. Chen et al. proposed the Trans-U-net, which inputs features extracted by a convolutional neural network encoder into a transformer to model global relationships, thereby enhancing the model's contextual understanding capabilities [10]. Cao et al. proposed the Swin-U-net, which incorporates a Hierarchical Self-Attention Mechanism and Shifted Window technique to improve feature extraction and processing efficiency [11]. While U-Net and U-Net++ are convolutional neural network-based models known for their lightweight parameters, they have limitations in capturing global image structure and context. In contrast, transformer architecture-based models, such as Trans-U-Net and Swin-U-net, utilize the transformer's ability to capture global information, making them particularly effective in computing long-distance dependencies. This enables more efficient feature learning and detailed recovery.

He et al. established a model to predict the outcome of ICIs using radiomic biomarkers as features, achieving an Area Under the Curve (AUC) of 0.81 [12]. In another study, He et al. classified the ICI outcomes in NSCLC patients into disease progression and partial response using CT image features, achieving AUC values of 0.78 and 0.81, respectively [13]. Shen et al. extracted ten texture feature sets to predict efficacy, resulting in an AUC of 0.81 [14]. Gong et al. combined 1,118 CT radiomic features to predict ICI efficacy, achieving an AUC of 0.82 [15]. These studies demonstrate the effectiveness of imaging data in predicting treatment outcomes. However, they primarily focused on medical image data from a single time point, overlooking the temporal changes in tumor characteristics. Additionally, these studies did not incorporate patients' biological indicators. Combining imaging data with biological and clinical indicators offers a more comprehensive assessment of a patient's overall health.

This study presents an improved U-Net segmentation model based on Efficient Channel Attention (ECA) to accurately segment the lesion regions of interest in CT images [16]. The proposed prediction model combines radiomic features from chest CT images and biological indicator features collected from two time points, before and after immunotherapy. Feature dimensionality reduction and selection were performed using LDA and Pearson algorithms, and a SVM was employed to establish the prediction model [17-19].

Materials and methods

Materials

This study was approved by the Ethics Committee of Shanghai Chest Hospital (Ethics approval number: KS24074). The research included 427 pairs of pre- and post-treatment CT images and biological markers (12 biomarkers, including white blood cell count and neutrophil count) from 103 NSCLC patients [20, 21]. Lesions were annotated by two senior radiologists, while treatment efficacy was assessed by one senior radiologist and one senior pulmonologist according to the RECIST 1.1 criteria. Efficacy was categorized into three types: partial response, stable disease, and progressive disease [22, 23].

Methods

The overall workflow of this study is illustrated in **Figure 1**. The proposed segmentation model was employed to segment lesions, followed by extraction of various features from CT images. Biological features were also collected from clinical test reports of the patients. Feature selection and dimensionality reduction were then performed to identify the features sensitive to predicting immunotherapy efficacy. Finally, the processed features were input into an SVM classifier to predict the immunotherapy outcome for the patients.

Lesion segmentation model

An improved segmentation model, named the Multi-Size Self-Attention model (MSSA) is proposed in this study. The workflow is illustrated in **Figure 2**. We employed a multi-size self-attention learning module based on the ECA module, which is embedded after every two 3x3 convolutional layers in the encoder. Additionally, a prompt-based cropping module that uses the mouse-clicks as prior knowledge was incorporated into the MSSA.

Multi-scale self-attention module

The multi-scale self-attention module employs a two-layer structure. Initially, the original feature map is divided into sub-feature maps, each with half the original size. These sub-feature maps are then processed using the multi-head self-attention mechanism to compute pixel-wise associations in both local

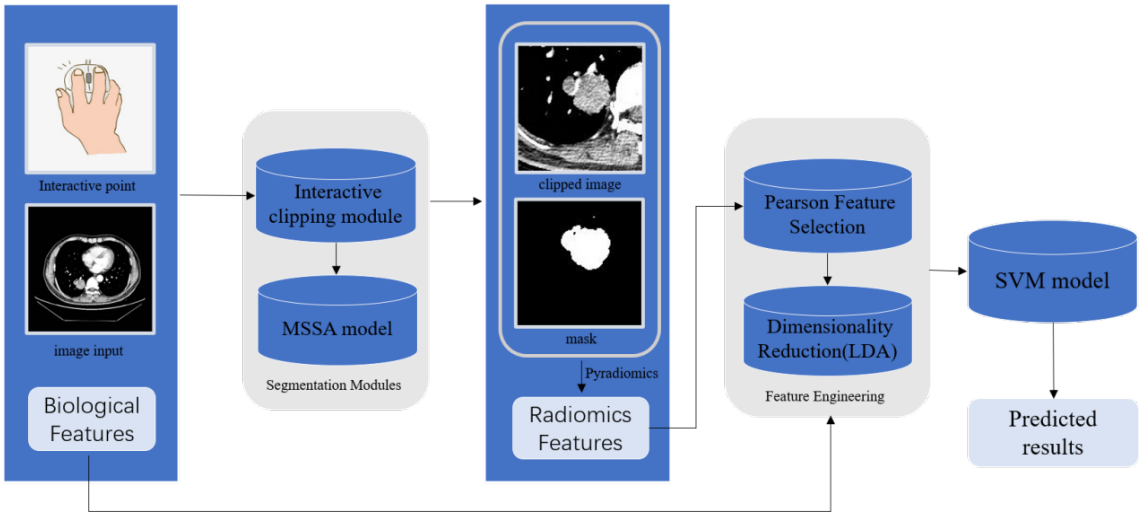

Figure 1. Overview of the prediction framework. The framework consists of three main modules: segmentation, feature engineering, and prediction. The segmentation module segments the lesion regions of interest, which are then input into PyRadiomics to extract radiomic features. These features undergo feature selection and dimensionality reduction, which are combined with biological features for further dimensionality reduction. Finally, the processed features are input into the SVM model.

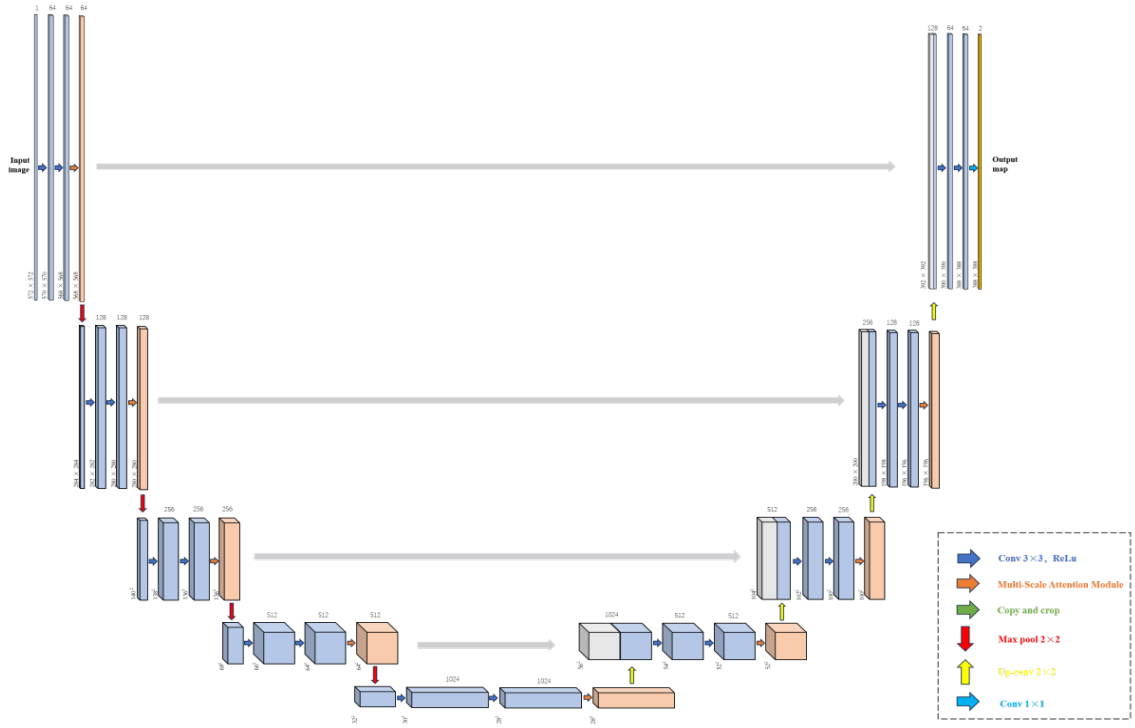

Figure 2. The architecture of the proposed MSSA. Blue boxes correspond to a multi-channel feature maps; Orange boxes refer to feature maps processed by the Multi-Size Self-Attention Learning Block; White boxes represent copied feature maps; Arrows denote different operations.

and global regions. The resulting pixel features are further processed by the ECA module, which enhances key features by weighting each channel. Afterward, the processed sub-feature maps are concatenated back to their original size, producing a weighted feature map. This weighted feature map is then divided into sub-feature maps, each with one-fourth of the original size, and the aforementioned operations are repeated. This method is particularly effective for lesion segmentation in lung CT images, addressing issues such as boundary blurring and feature extraction difficulties, ultimately achieving more precise segmentation. The diagram is shown in **Figure 3**.

The multi-head self-attention mechanism

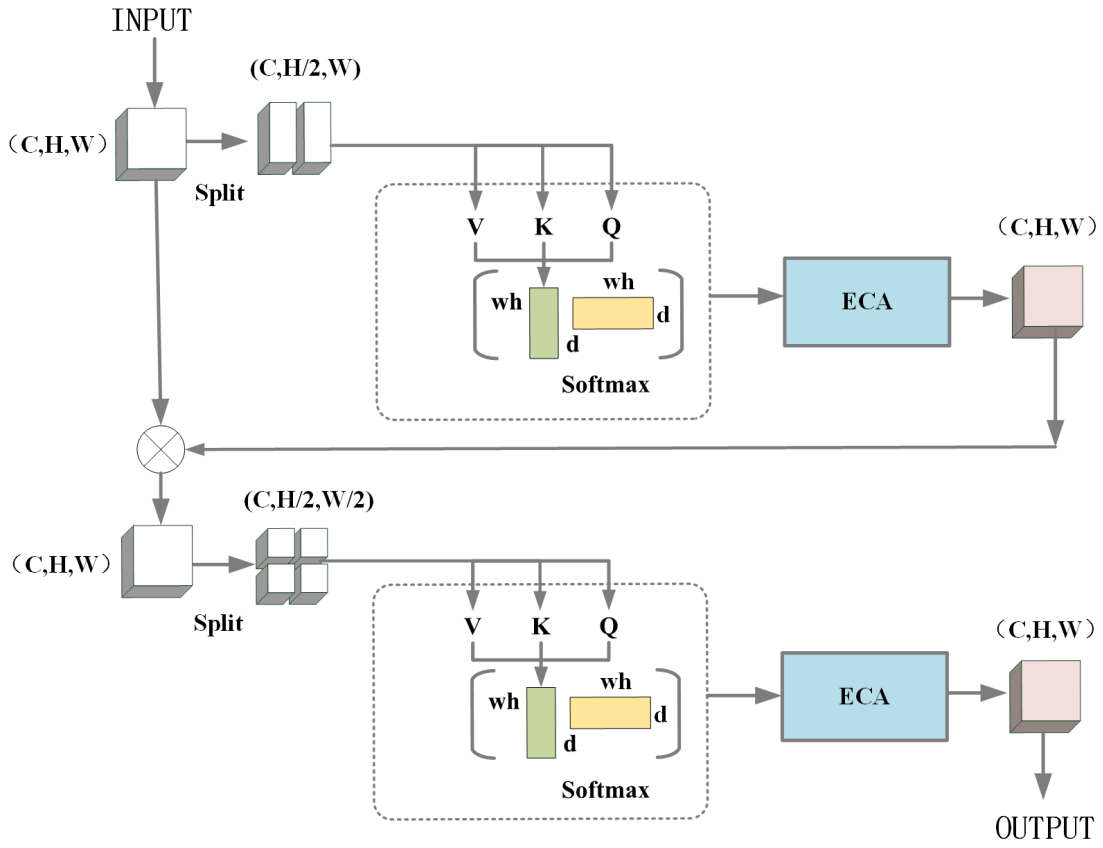

Figure 3. Schematic diagram of the multi-scale self-attention learning module (H, W, and C represent the height, width, and channel dimensions of the feature map, respectively). The input feature map is divided into 2 sub-feature maps of half size and then sequentially fed into the multi-head self-attention module and Efficient Channel Attention (ECA) module. Subsequently, the sub-feature maps are concatenated back to the original size. Following this, the resulting feature map is further divided into 4 sub-feature maps of one-quarter size, and the aforementioned process is repeated.

generates weight matrices w_g , w_k and w_v based on the similarity relationships between pixels [24]. Then, the query matrix (Q), key matrix (K), and value matrix (V) are obtained according to Equation (1):

$$\begin{aligned} Q &= W_g \cdot X \\ K &= W_k \cdot x \\ V &= W_v \cdot x \end{aligned} \quad (1)$$

Thus, the mathematical expression of the self-attention mechanism is:

$$\sum_{i=1}^{N} \left[\mathrm{Softmax}\left(\frac{\exp(s_i)}{\sum_{j=1}^{N}} \exp(s_j) \right) \cdot \boldsymbol{V}_i \right]; s_i = \frac{QK_i^T}{\sqrt{d}} \quad (2)$$

Where: N represents the maximum index value within the matrix; Si denotes the similarity between Q and K; Vi represents the value indexed by i in V; and d is the dimension of Q and K. Following the self-attention mechanism, an ECA module is incorporated. The ECA module utilizes a linear transformation combined with global average pooling, offering lower computational complexity compared to other channel attention mechanisms. **Figure 4** illustrates the corresponding schematic diagram:

First, global average pooling is applied to the feature map, as shown in Equation (3):

$$\mathrm{GAP}(\boldsymbol{U}) = \frac{1}{W \times H} \sum_{i=1,j=1}^{WH} U_{i,j} \quad (3)$$

Then, convolution operations are performed on *GAP(X)* using a dynamic 1D convolutional kernel of size k to learn the importance weights between different channels. The definition of the convolution kernel adaptive function and weights ω∈R1×1×C is as follows:

$$k = \psi(C) = \left| \frac{\log_2(C)}{\gamma} + \frac{b}{\gamma} \right|_{\mathrm{odd}} \quad (4)$$

$$\boldsymbol{\omega} = \mathrm{Sigmoid}\left(\mathrm{ClD_k}\left(\mathrm{GAP(U)} \right) \right) \quad (5)$$

Where, in Equation (4), k represents the convolutional kernel size, $|.|_{\mathrm{odd}}$ ensures that k is an odd number, and γ and b are used to adjust the ratio between C and k ; in Equation (5), the vector ω adjusts the attention

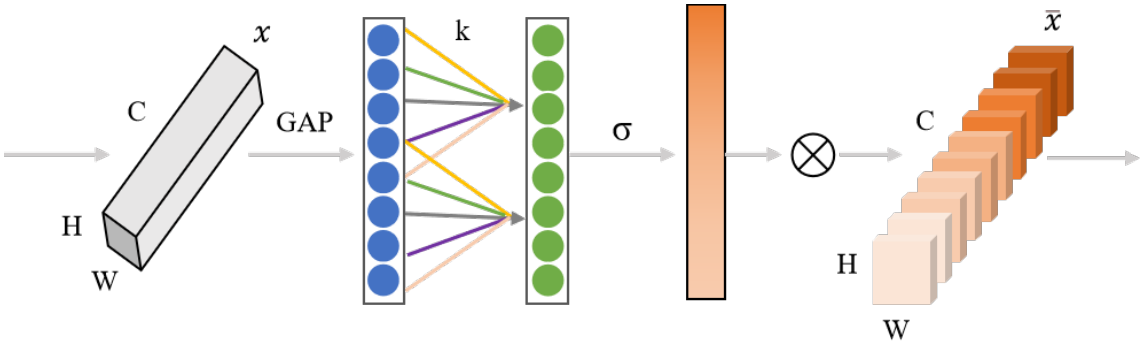

Figure 4. Schematic diagram of the Efficient Channel Attention (ECA) mechanism. X represents the input feature map. First, global average pooling (GAP) is performed, followed by a convolution using a 1D convolutional kernel of size k. σ denotes the Sigmoid activation function, represents element-wise multiplication, and is the weighted feature map. The features of each channel are adjusted according to their importance.

weights of each channel, and the Sigmoid function computes the activation values of the 1D convolution output. Finally, the generated weights are applied to the original feature map through element-wise multiplication, enhancing important channels while suppressing less important ones [25].

Prompt-based cropping module

In this module, a physician is required to perform a single click at the center of the lesion on any slice of the CT scan. The click point serves as the center, for cropping the CT image according to Equation (6), resizing the CT image to (128, 128) pixels, as illustrated in **Figure 4**. When processing 3D CT data, this interactive point is propagated to other CT slices via translation, allowing all CT slices to undergo the cropping operation.

$$\begin{aligned} X1 &= X - \frac{R}{2} \\ X2 &= X + \frac{R}{2} \\ Y1 &= Y - \frac{R}{2} \\ Y2 &= Y + \frac{R}{2} \\ \mathrm{Img} &*= \mathrm{Img}[X1{:}X2, Y1{:}Y2] \end{aligned} \tag{6}$$

Here, (*X, Y*) represents the coordinates of the interactive point provided by the physician, R is the size of the desired ROI to be cropped, and *X1, X2, Y1, Y2* are the horizontal and vertical coordinates after cropping. The brackets [] denote the slicing operation. To save labor, the interactive points in the training set are obtained based on the mask images.

Feature selection

Radiomic features were extracted from the CT images using the PyRadiomics tool. These features were then matched with the patient's data and the timing of the CT examinations. This resulted in a dataset of 427 pairs of 3D CT images from the same patient before and after treatment, comprising over 1,500 different feature differences. Two feature selection methods (Pearson and LASSO) were applied to this dataset to identify the top 21 radiomic features most relevant to treatment efficacy [26-29]. Furthermore, these selected features were combined with 12 biological features for Principal Component Analysis (PCA) and LDA, aiming to optimize the data representation [30, 31].

Outcome prediction

SVM was selected as the classification prediction model due to its strong ability in handling high-dimensional and nonlinear data. By maximizing the margin and utilizing kernel functions, SVM demonstrates excellent generalization performance and robustness against overfitting, making it widely used in the medical field as well as other domains [32-34].

Experiments and results

Experimental configuration

All experiments were conducted on a system equipped with an Intel i12-12700KF processor, Nvidia RTX 3090 GPU, and 16 GB of memory. The software configuration included Python 3.9 and PyTorch 1.8. The dataset was split into training and testing sets in an 8:2 ratio. For the segmentation model, stochastic gradient descent was chosen as the optimizer, with a batch size of 9, an initial learning rate of 0.001, and a total of 100 iterations. The loss function combined binary cross-entropy and Dice loss (BCE-Dice-Loss). Due to the high computational cost, 5-fold cross-validation was employed

Table 1. Comparison of Segmentation Performance of Various Models on the Test Set

Methods/ Evaluation Metrics		IoU (%)	PPV (%)	Dice (%)	HD_95
U-net*		78.92±1.52	85.58±1.31	86.26±1.52	2.35±0.51
U-net++*		78.52±1.12	85.21±1.46	86.34±1.23	2.85±0.56
Swin-U-net*		79.82±1.58	86.27±1.71	87.06±1.12	2.23±0.36
Trans-U-net*		79.12±1.62	85.63±1.43	86.45±1.01	2.09±0.41
MSSA		80.08±1.27	88.86±1.12	88.40±0.95	2.21±0.43
Incorporation of Prompt-based Cropping Module	U-net*	79.85±1.34	87.92±1.01	87.85±1.82	2.33±0.53
	U-net++*	79.23±1.29	87.12±1.89	87.26±1.43	2.62±0.51
	Swin-U-net*	80.23±1.45	88.51±1.27	88.05±1.32	2.35±0.56
	Trans-U-net*	80.28±1.04	88.11±1.81	88.29±1.27	2.07±0.58
	MSSA	82.15±1.02	89.23±1.04	90.09±1.28	2.18±0.31

Note: * Indicates significant difference compared to MSSA model. IoU, Intersection over Union; PPV, Positive Predictive Value.

Table 2. Comparison of Segmentation Performance in Ablation Experiments for Different Models

Baseline Model	Module1	Module2	IoU (%)	PPV (%)	Dice (%)	Hd_95
√			78.92±1.52	85.58±1.31	86.26±1.52	2.15±0.51
√	√		80.08±1.27	88.86±1.12	88.40±0.95	2.86±0.31
√		√	79.85±1.34	87.92±1.01	87.85±1.82	2.33±0.53
√	√	√	82.15±1.02	89.23±1.04	90.09±1.28	2.18±0.43

Note: IoU, Intersection over Union; PPV, Positive Predictive Value.

to evaluate segmentation performance, balancing computational efficiency with evaluation reliability. The classification model SVM was trained and tested using the Scikit-learn package in Python and its performance was evaluated using 10-fold cross-validation, providing fine-grained and robust evaluation with relatively low computational burden [35].

Results

Lesion segmentation model

The upper part of **Table 1** presents the performance of various models on the lung lesion segmentation task. The U-Net network, serving as the baseline model, achieved a Dice coefficient of 86.26%. The best-performing comparison model was the Swin-U-Net, with a Dice coefficient of 87.06%. Our proposed method, MSSA, achieved an intersection over union (IoU) of 80.08%, positive predictive value (PPV) of 88.86%, and Dice coefficient of 88.40%, outperforming all other models.

The lower part of **Table 1** shows the performance of each model after incorporating the prompt-based cropping module. All models exhibited an improvement of over 1% in the dice coefficient. Notably, the MSSA model achieved an outstanding dice coefficient of 90.09%, representing a performance improvement of 6.72% compared to the baseline U-Net model.

Ablation experiments of segmentation model

Table 2 presents a comparison of segmentation performance for models derived from the base U-Net network, incorporating different combinations of two modules (Module 1: Multi-scale Self-attention Learning Module and Module 2: Prompt-based Cropping Module). Incorporating the Multi-scale Self-attention Learning Module improved the model's IoU, PPV, and Dice coefficient by 1.45%, 3.83% and 2.71%, respectively. Adding the Prompt-based Cropping Module further enhanced IoU, PPV and Dice coefficient by 1.19%, 2.73% and 1.84%, respectively. When both modules were integrated, the model's IoU, PPV and Dice coefficient are improved by 4.09%, 4.27% and 4.44%, respectively. These results validate that the combined use of both modules significantly enhances segmentation performance.

Table 3. Outcome Prediction Results with Different Data and Feature Selection Combinations

Feature Data	Feature Engineering	AUC (%)	Accuracy (%)	Sensitivity (%)	Specificity (%)	PPV (%)
Data-A	Lasso + PCA	49.41±8.22	51.13±3.20	35.32±2.79	42.32±1.25	33.68±17.59
	Lasso + LDA	47.10±11.85	54.80±10.83	77.87±10.06	20.90±7.07	59.47±14.86
	Pearson +PCA	61.31±15.52	61.24±10.60	43.31±21.21	75.52±13.20	56.01±14.22
	Pearson +LDA	58.17±5.78	52.54±5.83	38.46±5.32	69.67±3.84	44.84±15.28
Data-B	Lasso + PCA	67.53±13.87	60.17±7.91	38.49±13.96	81.40±8.57	60.49±17.29
	Lasso + LDA	78.26±10.27	69.41±9.01	80.12±8.97	60.93±16.72	68.90±16.39
	Pearson +PCA	72.26±9.06	63.73±9.40	53.01±13.28	74.83±12.57	58.45±14.39
	Pearson +LDA	78.97±9.39	69.04±7.99	62.24±9.67	78.66±11.21	65.43±13.68
Data-C	Lasso + PCA	74.44±5.23	66.93±6.96	52.00±14.67	78.37±6.89	63.27±11.17
	Lasso + LDA	82.24±6.13	75.85±7.54	66.94±12.88	82.88±4.07	73.91±4.97
	Pearson +PCA	81.83±6.28	75.84±8.71	66.30±14.27	83.51±7.08	75.23±8.72
	Pearson +LDA	85.63±9.67	77.60±9.93	73.52±8.90	81.68±7.29	74.62±9.42

Note: PCA, Principal Component Analysis; LDA, Linear Discriminant Analysis; PPV, Positive Predictive Value.

Feature selection and outcome prediction

To evaluate the performance of the model, this study employed three groups of data:

Data-A: Radiomic features derived solely from the first period CT images of patients.

Data-B: Radiomic features from both the first and second period CT images.

Data-C: Radiomic features from both periods combined with biological features.

For each data group, two feature selection methods (Pearson and LASSO) and two feature dimensionality reduction methods (PCA and LDA) were applied in various combinations. The experimental results are shown in **Table 3**, with all prediction models using SVM for classification. The optimal feature selection scheme was identified as using Pearson and LDA. The final results for specificity, sensitivity, AUC, accuracy, and precision reached 85.63%, 77.60%, 73.52%, 81.68% and 74.62%, respectively. Notably, sensitivity, AUC, and accuracy outperformed other feature combinations.

Comparing Data-A and Data-B, experiments based solely on radiomic features from pre- and post-treatment CT images significantly outperform those based on a single-period CT image across all evaluation metrics. This highlights the superiority of using multi-period CT images. When comparing Data-B and Data-C, it was observed that the combination of radiomic and biological features consistently yielded better predictive performance over radiomic features alone, regardless of the feature engineering technique used. This indicates that combining radiomic and biological features provides a more effective strategy for predicting the efficacy of immunotherapy for lung cancer patients.

Ablation experiments on outcome prediction

Table 4 presents the comparison of classification performance for models based on the baseline SVM, using a dataset containing radiomic features from two-period CT images and biological features. Incorporating the Pearson feature selection method improved the model's AUC and Accuracy by 62.62% and 27.96%, respectively. Adding the LDA feature dimensionality reduction method resulted in an improvement in AUC and accuracy by 64.52% and 23.43%, respectively. When both methods are applied simultaneously, the AUC and accuracy increased by 81.80% and 41.61%, respectively, demonstrating that the incorporation of these feature engineering techniques can significantly enhance classification performance.

Discussion

This study proposes a method for predicting the efficacy of immunotherapy in lung cancer, leveraging pre- and post-treatment CT images.

Table 4. Ablation Experiment Results for Outcome Prediction

Baseline Model	Pearson	LDA	AUC (%)	Accuracy (%)	Sensitivity (%)	Specificity (%)	PPV (%)
√			47.10±11.85	54.80±10.83	77.87±10.06	20.90±7.07	59.47±14.86
√	√		76.62±6.82	70.12±5.46	63.42±10.72	75.92±7.98	66.18±9.45
√		√	77.49±12.94	67.64±12.96	64.34±11.92	77.56±8.50	63.06±12.83
√	√	√	85.63±9.67	77.60±9.93	73.52±8.90	81.68±7.29	74.62±9.42

Note: LDA, Linear Discriminant Analysis; AUC, Area under the curve; PPV, Positive Predictive Value.

It combines an improved U-Net segmentation model, radiomic feature extraction, and clinical biological indicators to achieve precise predictions of immunotherapy outcomes for NSCLC patients.

In terms of lesion segmentation, we introduced a multi-scale self-attention learning module based on ECA. This module enhances the model's ability to identify lesion areas by performing self-attention computation and channel weighting at multiple scales. The experimental results show that the improved MSSA model outperforms some existing popular segmentation models across four evaluation metrics, including the Dice coefficient. Particularly, after integrating the prompt-based cropping module, the Dice coefficient reached 90.09%, significantly improving the segmentation accuracy. This improvement not only facilitates more precise extraction of radiomic features from lesion areas but also provides a reliable foundation for subsequent efficacy predictions.

In constructing the predictive model, this study incorporated data from pre- and post-treatment CT images, along with relevant clinical biological indicators. Using feature engineering methods like Pearson correlation analysis and LDA dimensionality reduction, we selected the most relevant feature combinations associated with treatment efficacy. The experimental results showed that models combining radiomic features from pre- and post-treatment CT images and biological features outperformed models relying solely on single-period CT images or those without biological features in terms of AUC, accuracy, sensitivity and specificity. This suggests that dynamic information on tumor changes during treatment, coupled with the clinical state of patients, plays a crucial role in predicting treatment efficacy, thereby offering more comprehensive and accurate predictive results.

Despite the achievements of this study, several limitations should be acknowledged. First, the sample size is relatively small and primarily drawn from a single center, which may limit the generalizability of the model. Future studies should validate and refine the model using larger, multi-center datasets. Second, the current research focuses predominantly on NSCLC patients. The applicability of the model to other types of lung cancer or its potential for predicting immunotherapy efficacy in other cancers remains to be explored.

Conclusion

This study proposes a method for predicting the outcome of immunotherapy in lung cancer patients based on pre- and post-treatment CT images. By integrating the proposed segmentation model, radiomic feature extraction, and clinical biological indicators, the method provides accurate predictions of immunotherapy efficacy in NSCLC patients. The proposed segmentation model outperforms existing popular methods, providing an effective solution for CT lesion segmentation in NSCLC. The prediction model achieves specificity, sensitivity, AUC, accuracy, and precision rates of 85.63%, 77.60%, 73.52%, 81.68%, and 74.62%, respectively. These results provide new insights into predicting immunotherapy efficacy in NSCLC, enhancing the scientific basis for medical decision-making. This method shows strong potential for broad application in clinical application, offering oncologists more precise and effective diagnostic and treatment support.

Author contributions: Wensong Yan was responsible for conceptualization, methodology, and writing of the original draft. Shiju Yan provided supervision, offered technical guidance, and contributed to review and editing. Yunhua Xu handled data collection and offered medical guidance. All authors have read and agreed to the final version of the manuscript.

References

[1] Hendriks LE, Remon J, Faivre-Finn C, et al. Non-small-cell lung cancer. Nat Rev Dis Primers 2024;10(1):71
[2] Lahiri A, Maji A, Potdar PD, et al. Lung cancer immunotherapy: progress, pitfalls, and promises. Mol Cancer 2023;22(1):40.
[3] Hsieh K, Dickstein DR, Runnels J, et al. Radiotherapy and immunotherapy in lung cancer. Biomedicines 2023;11(6):1642.
[4] Khadela A, Postwala H, Rana D, et al. A review of recent advances in the novel therapeutic targets and immunotherapy for lung cancer. Med Oncol 2023;40(5):152.
[5] Pan Y, Fu Y, Zeng Y, et al. The key to immunotherapy: how to choose better therapeutic biomarkers for patients with non-small cell lung cancer. Biomark Res 2022;10(1):9.
[6] John T, Sakai H, Ikeda S, et al. First-line nivolumab plus ipilimumab combined with two cycles of chemotherapy in advanced non-small cell lung cancer: a subanalysis of Asian patients in CheckMate 9LA. Int J Clin Oncol 2022;27(4):695-706.
[7] Yin X, Liao H, Yun H, et al. Artificial intelligence-based prediction of clinical outcome in immunotherapy and targeted therapy of lung cancer. Semin Cancer Biol 2022;86(Pt 2):146-159.
[8] Ronneberger O, Fischer P, Brox T. U-Net: Convolutional Networks for Biomedical Image Segmentation. Medical Image Computing and Computer-Assisted Intervention - MICCAI 2015 2015;234-241.
[9] Zhou Z, Rahman Siddiquee MM, Tajbakhsh N, et al. Unet++: A nested u-net architecture for medical image segmentation. Deep Learning in Medical Image Analysis and Multimodal Learning for Clinical Decision Support 2018;3-11.
[10] Chen J, Lu Y, Yu Q, et al. Transunet: Transformers make strong encoders for medical image segmentation. arXiv preprint arXiv:2102.04306 2021.
[11] Cao H, Wang Y, Chen J, et al. Swin-unet: Unet-like pure transformer for medical image segmentation. European conference on computer vision 2022;205-218.
[12] He B, Dong D, She Y, et al. Predicting response to immunotherapy in advanced non-small-cell lung cancer using tumor mutational burden radiomic biomarker. J Immunother Cancer 2020;8(2):e000550.
[13] He B-X, Zhong Y-F, Zhu Y-B, et al. Deep learning for predicting immunotherapeutic efficacy in advanced non-small cell lung cancer patients: a retrospective study combining progression-free survival risk and overall survival risk. Transl Lung Cancer Res 2022;11(4):670-685.
[14] Shen L, Fu H, Tao G, et al. Pre-immunotherapy contrast-enhanced CT texture-based classification: a useful approach to non-small cell lung cancer immunotherapy efficacy prediction. Front Oncol 2021;11:591106.
[15] Gong J, Bao X, Wang T, et al. A short-term follow-up CT based radiomics approach to predict response to immunotherapy in advanced non-small-cell lung cancer. Oncoimmunology 2022;11(1):2028962.
[16] Wang Q, Wu B, Zhu P, et al. ECA-Net: Efficient channel attention for deep convolutional neural networks. Proceedings of the IEEE/CVF conference on computer vision and pattern recognition 2020;11534-11542.
[17] Jelodar H, Wang Y, Yuan C, et al. Latent Dirichlet allocation (LDA) and topic modeling: models, applications, a survey. Multimed Tools Appl 2019;78:15169-15211.
[18] Cleophas TJ, Zwinderman AH. Bayesian Pearson Correlation Analysis. In: Cleophas TJ, Zwinderman AH, editors. Modern Bayesian Statistics in Clinical Research. Cham (SWITZERLAND). Springer International Publishing, 2018. p. 111-118.
[19] Wang H, Zhou W, Shao Y. A new fast ADMM for kernelless SVM classifier with truncated fraction loss. Knowl-Based Syst 2024;283:111214.
[20] Benzekry S, Grangeon M, Karlsen M, et al. Machine learning for prediction of immunotherapy efficacy in non-small cell lung cancer from simple clinical and biological data. Cancers 2021;13:6210.
[21] Mariam A, Kamath S, Schveder K, et al. Large-Scale Meta-Analysis of Potential Biomarkers for Treatment Response to Anti-PD-1/PD-L1 Immune Checkpoint Inhibitors. medRxiv 2020;2020.2011.
[22] Sun C, Ma X, Meng F, et al. Tumor microenvironment (TME) and single-source dual-energy CT (ssDECT) on assessment of inconformity between RECIST1. 1 and pathological remission in neoadjuvant immunotherapy of NSCLC. Neoplasia 2024;50:100977.
[23] He LN, Chen T, Fu S, et al. Reducing number of target lesions for RECIST1. 1 to predict survivals in patients with advanced non-small-cell lung cancer undergoing anti-PD1/PD-L1 monotherapy. Lung Cancer 2022;165:10-17.
[24] Zhong Y, Tang Z, Zhang H, et al. A froth image segmentation method via generative adversarial networks with multi-scale self-attention mechanism. Multimed Tools Appl 2024;83:19663-19682.
[25] Tian Q, Wang Z, Cui X. Improved Unet brain tumor image segmentation based on GSConv module and ECA attention mechanism. arXiv preprint arXiv:2409.13626 2024.

[26] Rahadian H, Bandong S, Widyotriatmo A, et al. Image encoding selection based on Pearson correlation coefficient for time series anomaly detection. Alex Eng J 2023;82:304-322.

[27] James G, Witten D, Hastie T, et al. An Introduction to Statistical Learning: with Applications in Python. Cham (SWITZERLAND). Springer International Publishing, 2023. p. 69-134.

[28] Antoniadis A, Lambert-Lacroix S, Poggi J-M. Random forests for global sensitivity analysis: A selective review. Reliab Eng Syst Safe 2021;206:107312.

[29] Ghosh P, Azam S, Jonkman M, et al. Efficient prediction of cardiovascular disease using machine learning algorithms with relief and LASSO feature selection techniques. IEEE Access 2021;9:19304-19326.

[30] Kurita T. Principal Component Analysis (PCA). In: Ikeuchi K, editors. Computer Vision: A Reference Guide. Cham (SWITZERLAND). Springer International Publishing, 2021. p. 1013-1016.

[31] Egwom OJ, Hassan M, Tanimu JJ, et al. An LDA–SVM machine learning model for breast cancer classification. BioMedInformatics 2022;2(3):345-358.

[32] Shanmugam S, Dharmar S. Implementation of a non-linear SVM classification for seizure EEG signal analysis on FPGA. Eng Appl Artif Intell 2024;131:107826.

[33] Alqhtani SM, Soomro TA, Shah AA, et al. Improved Brain Tumor Segmentation and Classification in Brain MRI With FCM-SVM: A Diagnostic Approach. IEEE Access 2024;12:61312-61335.

[34] Hoque R, Billah M, Debnath A, et al. Heart disease prediction using SVM. Int J Sci Res Arch 2024;11:412-420.

[35] Zhang X, Liu C-A. Model averaging prediction by K-fold cross-validation. J Econom 2023;235:280-301.